Applied Catalysis B: Environmental 163 (2015) 330–342

Contents lists available at ScienceDirect

Applied Catalysis B: Environmental

journal homepage: www.elsevier.com/locate/apcatb

Optimization and mechanism elucidation of the catalytic photo-degradation of the dyes Eosin Yellow (EY) and Naphthol blue black (NBB) by a polyaniline-coated titanium dioxide nanocomposite

Sushanta Debnath[a,*], Niladri Ballav[a], Hlengilizwe Nyoni[a], Arjun Maity[b,c,**], Kriveshini Pillay[a,***]

[a] Department of Applied Chemistry, University of Johannesburg, Johannesburg, South Africa
[b] National Centre for Nano-structured Materials, Council of Scientific and Industrial Research, Pretoria, South Africa
[c] Department of Civil and Chemical Engineering, University of South Africa (UNISA), South Africa

ARTICLE INFO

Article history:
Received 25 May 2014
Received in revised form 31 July 2014
Accepted 7 August 2014
Available online 15 August 2014

Keywords:
Photocatalytic degradation
Eosin Yellow, Naphthol blue black
Polyaniline coated titanium oxide nanocomposite
Response Surface Methodology

ABSTRACT

A polyaniline-coated titanium oxide nanocomposite (PTO) was synthesized, characterized and used in the catalytic photo-degradation of the anionic dyes Eosin Yellow (EY) and Naphthol blue black (NBB). An emphasis was placed on the key parameters governing the degradation process. It was noted that the extent of degradation was higher at lower pH for both dyes. The rate of degradation of both dyes also increased with increasing catalyst dosage, Langmuir–Hinselwood models and other second-order kinetic models verified that heterogeneous photocatalysis occurred. The rate of degradation increased with increasing initial dye concentrations and only increased gradually with an increase in UV light intensity in the absence of the catalyst. The optimum operating conditions for the degradation was also predicted using response surface methodology (RSM) analysis as a statistical tool. This analysis revealed that the initial dye concentration, pH and dosage of the catalyst are all significant parameters in the degradation process. The combined effect of pH and initial concentration was antagonistic whilst the combined effect of initial concentration and catalyst dosage and the combined effect of catalyst dosage and pH were both synergistic. The optimum degradation percentages were found to be 99.85 and 99.74 for EY and NBB respectively. These optimum percentage degradations were observed at pH 3.0, initial dye concentration 15 mg L^{-1} and a catalyst dosage of 1.0 g L^{-1}. LC–MS data was also used to identify the photodegradation products and to propose a mechanism of photodegradation.

1. Introduction

Textile dyes and other dyestuffs, which are used in industrial applications like paper and pulp, adhesives, art supplies, beverages, ceramics, cosmetics, food, paints, etc., constitute a class of compounds, which increases the environmental pollution load largely. Among the dyes, the azo-class of dyes with aromatic moieties linked with azo bond (—N=N—) acquires the majority of the share (50–70%) of the dyes used in textile and other industries [1,2]. About 1–20% of the used dye remains unfixed and the same is discharged in the waste effluent causing the coloration of the wastewater and threat to the aquatic life [3,4]. The dyes itself and its degradation products are highly carcinogenic and mutagenic [5–9]. Thus, removal of the dye and their degraded products is highly essential in view of the environmental hazard that this poses as well as the threat to human health.

Reactive dyes are highly soluble in water and their removal from aqueous solution by conventional coagulation and filtration, activated sludge processes, adsorption, biological treatment, chlorination, ozonation, flocculation, reverse osmosis are insufficient for the wastewater treatment either for not being cost-effective or not being destructive enough [10–16]. The non-destructive processes only transfer the pollutant from one phase to another, which further requires treatment and a different kind of pollution is faced. The advance oxidation process (AOP) is one of the treatment methods, which have been extensively studied [17–19]. AOPs are based

* Corresponding author. Tel.: +27 11 5596128; fax: +27 11 5596425.
** Corresponding author at: National Centre for Nano-structured Materials, Council of Scientific and Industrial Research, Pretoria, South Africa. Tel.: +27 12 8412658; fax: +27 12 8412229.
*** Corresponding author. Tel.: +27 11 5596128; fax: +27 11 5596425.
E-mail addresses: sushanta.debnath@yahoo.com, debnath.sushanta@gmail.com (S. Debnath), AMaity@csir.co.za (A. Maity), kriveshinip@uj.ac.za (K. Pillay).

http://dx.doi.org/10.1016/j.apcatb.2014.08.011
0926-3373/

on the generation of hydroxyl radicals ($OH^{\bullet}$) which are very active in degrading different classes of organic pollutants [20,21].

With comparison to the AOPs, heterogeneous photocatalysis is considered as a cost-effective and environment friendly alternative for the refinement of the dye containing wastewater [22,23]. The use of TiO_2 (TO) and its composites under UV irradiation has been extensively studied for degrading and mineralizing of reactive dyes from dye containing solutions [11,24–28]. TiO_2 based materials are good photocatalysts due to low band gap energy of TiO_2 compared to other photocatalysts. Some TiO_2 based photocatalysts reported by other authors are $SrTiO_3$ composite [29], CdS embedded TiO_2 nano-spheres [30], $AgAlO_2/TiO_2$ composite [31], TiO_2/Ag composite [32], Cu doped TiO_2 thin film [33], etc. Photocatalysis does not require any oxidizing chemicals and can be operated at mild conditions of temperature and pressure.

The limitation of the photocatalysts lies in the existence of the partially degraded intermediates into the reaction solution which could not be removed by photocatalysis, or can be removed by prolonged UV irradiation only. This decreases the cost effectiveness of the process. To overcome this drawback, the photocatalyst could be coated with some compounds, which are able to remove the intermediates, by adsorption and as a result contaminant free final aqueous solution could be regained.

Most of the studies conducted to date do not report the interaction of all the independent variables used in the degradation studies. Response surface methodology (RSM) is the statistical tool which correlates the inter-dependent relation between the degradation process variables [34]. Based on some experimental data, RSM can optimize the degradation process. To date, no correspondences are known to establish the optimization of degradation of Eosin Y (EY) and Naphthol blue black (NBB) by polyaniline coated TiO_2 (PTO) applying the RSM.

In this communication, we have used a PTO nanocomposite for the degradation of two dyes, EY and NBB from their aqueous solution. The parameters varied are the pH, catalyst dose, initial dye concentration and UV light intensity. The results are analyzed using degradation kinetic parameters e.g. Langmuir–Hinshelwood equation and second order equation. Three factor central composite design (CCD) combined with RSM is applied to optimize the response as the degradation percentage of EY and NBB using PTO (photocatalyst dosage, pH and the initial dye concentration is varied during the degradation). Finally, the degraded products were identified by LCMS study and a mechanism of degradation was proposed based on the LCMS results.

2. Materials and methods

2.1. Reagents

EY (M.W. 647.89, $C_{20}H_8Br_4O_5$) and NBB (M.W. 616.49, $C_{22}H_{14}N_6Na_2O_9S_2$) used in the preparation of synthetic dye stock solutions were purchased from Sigma Aldrich. The molecular structure of EY and NBB are given in Fig. S1 (Supplementary materials). The working solutions with known dye concentrations were thereafter prepared by diluting the stock solution using distilled water. Titanium(IV) oxide (TO) nanoparticles (21 nm) (Aeroxide^{TM}) (purity: 99.5%) and ammonium persulfate as an oxidant for aniline polymerization were also purchased from Sigma Aldrich. All other reagents used were of analytical grade.

2.2. Preparation of polyaniline coated titanium oxide (PTO) nanocomposite

Polyaniline (PANI) coated titanium oxide (PTO) composite was synthesized by in situ polymerization of aniline (ANI) monomer in presence of titanium dioxide (TO) nanoparticles. Five gram of TO was suspended in 500 mL 0.1 N HCl solution and stirred on a magnetic stirrer for 1 h. Thereafter, 1 mL of ANI was injected into the TO suspension and stirred for another 1 h to solubilize the ANI molecules. Finally, 10 mL of 1% (v/v) aqueous solution of ammonium persulfate (APS) was added to the suspension and stirred for overnight. The PANI coated TO particles were separated from the polymerization solution by means of filtration using 0.45 μm membrane filter and washed with acetone to remove the oligomers and unreacted monomers. The greenish mass was finally washed with double distilled water and dried at 60 °C under vacuum.

2.3. Instruments

The following instruments were used in the experimental work: (i) Thermo pH meter (model: Orion 4 star) for pH analysis, (ii) Rigaku X-ray diffractometer for the X-ray diffraction (XRD) analysis, (iii) Föurier Transform Infra Red (FTIR) spectrophotometer (Perkin Elmer (U.S.) Spectrum 100) for FTIR spectra, (iv) Micromeritics ASAP 2020 BET surface analyzer for surface area and pore size measurement (v) UV–visible spectrophotometer (Shimadzu 1800) for colorimetric analysis of the dyes and the diffuse reflectance spectrophotometry (vi) UV lamps (25 W and 15 W) for irradiation in the reactor was purchased from Philips and (vii) Waters 3100 HPLC/MS was used for LCMS of the degraded products

2.4. Experimental setup of the photo-reactor for degradation

The photodegradation of the EY and NBB dye was performed in an annular reactor as shown in the schematic diagram as Fig. 1. The dye solution was passed through the annular reactor using a peristaltic pump at different flow rates. The dye solution was stirred in a beaker using a magnetic stirrer to prevent the catalyst particles from settling down and to equilibrate the dye solution with the catalyst particles before entering the reactor. At a fixed time interval, 2 mL solution was collected from the sampling port and the residual dye concentration was measured using UV–visible spectrophotometer after filtering through 0.45 μM syringe filter. The parameters varied in the whole process are photocatalyst (PTO) dosage, pH and initial dye concentration in the reactor.

2.5. Actinometric determination of light intensity

The intensity of the irradiated light was measured by ferrioxalate actinometry. The potassium ferrioxalate was prepared by the method described by Hatchard and Parker [35]. In brief, 15 mL of 1.5 mM potassium oxalate was mixed with 5 mL of 1.5 mM $FeCl_3$ in a beaker. The greenish yellow precipitate of ferrioxalate was recrystallized three times from boiling water, collected after washing with cold water, and dried at 45 °C. The 0.01 M actinometer ferrioxalate solution was prepared by dissolving 2.947 g $K_3Fe(C_2O_4)_3$ in 1 L of 0.1 N H_2SO_4 solution. The dissolved Fe(II) was analyzed by 1,10 ortho-phenanthroline method [36]. The absorbance of the Fe(II)-O-Phen complex was measured in a 1 cm path length quartz cuvette at 510 nm. The calibration curve was constructed using 0.01, 0.02, 0.04, and 0.06 mM Fe^{2+} solution.

The 0.01 M actinometer ferrioxalate solution in 0.1 N H_2SO_4 was introduced into the same reactor as of the experimental one and the solution was irradiated with the lamps used for the photolysis of EY and NBB. Sampling of the irradiated solution was done at suitable interval and the amount of Fe^{2+} formed was determined from the calibration curve.

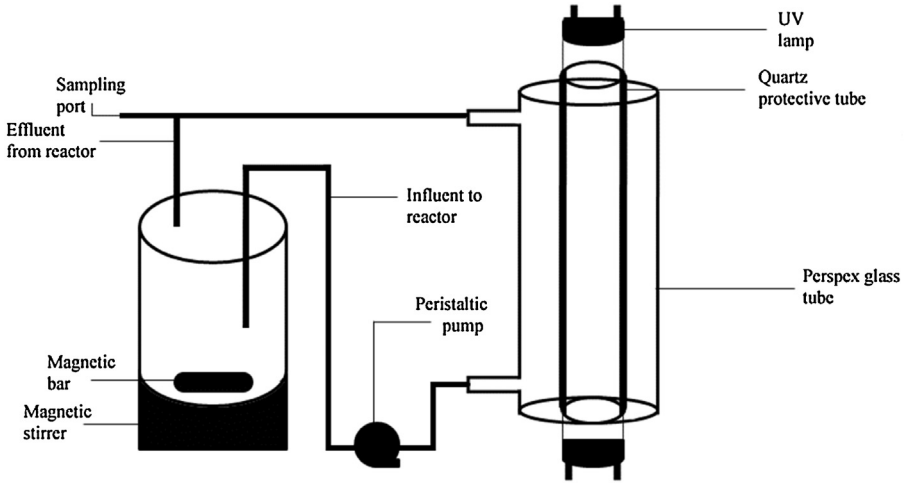

Fig. 1. Schematic diagram of the annular reactor used for degradation of EY and NBB with PTO.

2.6. Kinetic equations of degradation of EY and NBB by PTO

The kinetics of degradation was observed by subjecting the experimental points with kinetic models viz., second order and Langmuir Hinshelwood models.

The second order equation is given as [37],

$$C = \frac{C_o}{1 + k_2 C_o t} \quad (1)$$

where, k_2 (mg g^{-1} min^{-1}) is the second order rate constant and C_o and C (mg L^{-1}) are the dye concentration at initial and at time 't', respectively.

The Langmuir– Hinshelwood equation of heterogeneous catalysis is given as [38],

$$\ln\left(\frac{C}{C_o}\right) = -k_T k_a t = -k_{LH} t \quad (2)$$

$$k_{LH} = k_T k_a \quad (3)$$

The half life of the reaction is calculated from the equation,

$$t_{\frac{1}{2}} = \frac{0.693}{k_{LH}} \quad (4)$$

where k_T, k_a and k_{LH} (min^{-1}) are the specific reaction rate constant for the oxidation of the reactant, equilibrium constant of the reaction and the Langmuir– Hinshelwood model rate constant, respectively. C_o and C are the same as Eq. (1).

2.7. Response surface methodology (RSM) and data analysis

The RSM is a statistical analysis method which uses the quantitative data available from some experimental design and develops the regression model equations, which are useful in predicting and optimizing the operating conditions of some processes [34,39–46].

The mutual dependency of the variables, which influence the system, could be understood in this method. In this paper RSM is utilized to understand the interdependent relations between the operating variables in the degradation system, namely, initial concentrations of the dyes (EY and NBB), pH of the degradation system and mass of the photocatalyst (PTO).

This study was performed by employing the widely used standard RSM design—central composite experimental design (CCD). The chief advantage of using CCD study is to minimize the total number of experimental runs for determining the response effect. The CCD of this study is related to three numerical factors (center points) and one α value of 1.682. The CCD is considered of three independent variables: mass of the photocatalyst (m, g), concentration of the influent dye solution in the reactor (C, mg L^{-1}) and pH of the system. The observed response is the degradation efficiency of the dyes after 150 min (D, %). Three levels were assigned for all the independent variables and the coded variables (C, pH and m,) with the actual values and the response (D) are shown in Table 1. Total 20 runs were designed to run the system and a quadratic model was employed to investigate the interaction between the independent and the dependent variables [34].

$$Y = \beta_o + \sum \beta_i X_i + \sum \beta_{ii} X_i^2 + \sum \beta_{ij} X_i X_j$$

where, Y is the predicted response, β_o is the constant of the quadratic equation, β_i is the linear coefficient, β_{ii} is the squared coefficient and the β_{ij} is the cross product coefficient.

Analysis of the experimental data according to the RSM was performed using DESIGN EXPERT 7 software. The software was also employed to statistically evaluate the surfaces created according to the following criteria: (i) each variable must present a 'p'-value (the value of probability) less than 0.05 (<0.05) which implies that the term is significant at 95% confidence limit, (ii) the value of regression (R^2) should be closer to unity, which means that the predicted data are close to the real data points, (iii) the "lack of fit" must be significant ('p' < 0.05), which means that the model is adequate to describe the experimental data and eventually (iv) the residuals generated between the fitted data points and the experimental data points must present a normal distribution to validate the assumptions made by the *ANOVA* analysis [34].

3. Results and discussion

3.1. Characterization of the photo catalyst

3.1.1. Surface area and pore size

The BET surface area and the pore size distribution profile were determined by N_2 adsorption/desorption isotherm technique (Fig. S2: Supplementary materials). The degassing was done at 120 °C for 5 h and the analysis was done at –197.4 °C in a liquid nitrogen bath at an equilibration rate of 10 s. The BET surface area of PTO was found to be 49.81 m^2 g^{-1}. The surface area of the TO particles was reported to be 65 m^2 g^{-1} by the manufacturer [47]. Decrease in surface area after coating indicates increase in the size of the particles, which supports successful coating of TO by PANI. The average pore width of the composites was found to be 311.19 Å.

Table 1
Regression analysis and significance of the components in the quadratic model for EY and NBB degradation by PTO in presence of UV light.

Variables	Symbol	Factor code	Level of factors		
			−1	0	+1
Initial dye concentration ($mg\,L^{-1}$)	C_o	X_1	3.0	6.2	11
pH	pH	X_2	15	30	60
Adsorbent dosage ($g\,L^{-1}$)	m	X_3	0.25	0.50	1.0

Run	Coded levels			Observed degradation (%)		Predicted degradation (%)		Residual	
	X_1	X_2	X_3	EY	NBB	EY	NBB	EY	NBB
1	−1	−1	+1	99.85	99.74	96.76	98.20	−3.09	−1.54
2	−1	−1	−1	94.56	95.65	94.18	93.69	−0.38	−1.96
3	−1	0	0	98.91	99.66	100.7	99.62	1.84	−0.04
4	0	0	+1	98.93	99.11	97.36	95.18	−1.57	−3.93
5	+1	+1	+1	87.23	80.25	85.04	78.85	−2.19	−1.4
6	+1	−1	+1	95.68	98.56	98.59	99.05	2.91	0.49
7	0	0	0	98.91	96.93	98.29	94.77	−0.62	−2.16
8	+1	0	0	94.39	82.9	94.42	89.75	0.03	6.85
9	−1	+1	+1	85.32	87.54	89.26	91.73	3.94	4.19
10	0	0	0	98.91	96.93	98.29	94.77	−0.62	−2.16
11	0	0	0	98.91	96.93	98.29	94.77	−0.62	−2.16
12	0	0	0	98.91	96.93	98.29	94.77	−0.62	−2.16
13	−1	+1	−1	65.26	62.54	62.96	63.11	−2.3	0.57
14	0	0	−1	79.50	74.7	82.93	74.76	3.43	0.06
15	0	+1	0	81.33	80.06	78.55	78.94	−2.78	−1.12
16	+1	−1	−1	91.26	93.25	87.17	86.83	−4.09	−6.42
17	+1	+1	−1	46.56	41.26	49.89	42.52	3.33	1.26
18	0	0	0	98.91	96.93	98.29	94.77	−0.62	−2.16
19	0	−1	0	99.25	93.13	103.8	104.33	4.64	11.2
20	0	0	0	98.91	96.93	98.29	94.77	−0.62	−2.16

3.1.2. Diffuse reflectance spectroscopy

The diffuse reflectance spectrophotometry of TO and PTO were performed by using $BaSO_4$ as blank in an ISR-240A Integrating Sphere Attachment attached into the UV–visible spectrophotometer. The band gap energies of TiO_2 and PTO were calculated by plotting the values of $[F(R) \times h\upsilon]^n$ against the photon energy ($h\upsilon$). The value of 'n' depends on the type of the electronic transition which is 1 for direct and $\frac{1}{2}$ for indirect band gap of a semiconductor of crystalline nature [48].

The extrapolation of the tangent of the plot on x axis gives the band gap energy of the semiconductor. Fig. 2 shows the plot of $(K \times h\upsilon)^{1/2}$ versus $h\upsilon$ to calculate the band gap energy of TiO_2 and PTO. The band gap energies for TiO_2 and PTO are found to be 3.2 eV and 2.59 eV, respectively, which indicated PTO to be a better photocatalyst than the pure unmodified TiO_2. The π–π^* absorption in the polyaniline is much lower (1.7–2.3 eV) because the benzene rings are conjugated through an imine linkage. The experimental absorption spectrum for PANI shows a band gap of 1.5 eV which is interpreted as excitations to the polaron band [49,50]. It was reported that PANI is an efficient electron donor and good hole transporter upon light excitation [51]. In the combined system of PANI and TO (PTO), transfer of the electrons generated from the PANI upon UV-light irradiation to the conduction band (CB) of TO is thermodynamically favorable because, the LUMO of PANI is energetically higher than the CB of TO. As a result, interfacial charge transfer and separation between the PANI and the TO takes place and this could deliver a significant photo response to the UV light.

Upon coating of TO by PANI, the measured band gap energy (2.59 eV) of the hybrid composite is much lower than that of the pure TO (3.2 eV). The decrease in band gap is due to closeness of LUMO of PANI and the CB of the TO hence the radical generation is much more feasible in PTO than TO. On the other hand, higher pH_{zpc} of PTO favors the adsorption of the anionic dyes on the catalyst surface and as a result, a higher degree of photodegration is observed in case of PTO than TO. Due to these combined effects, relatively higher photoelectric conversion efficiency has been observed.

3.1.3. SEM and TEM image of PTO

The SEM image of PTO and TO with the EDS spectra are given in Fig. 3A and B, respectively. The SEM image of PTO indicates bigger particle size than the TO, which in turn confirms the coating of the TO particles with PANI, hence increasing in the size. The EDS analysis with weight percentage of constituent elements indicates presence of C, N, O and Ti which is the indication of successful compositing of the TiO_2 particles with PANI, whereas, the EDS of the TO only contains Ti and O. The globular coated particles are also visible in the SEM image.

As shown in Fig. 3C, TEM images of the PTO composites are of irregular shape with PANI backbone embedded with TO nanoparticles. This suggests the successful coating of TO by PANI. The average TO nanoparticles sizes are in the range of 15–25 nm with interlattice distance of 0.34 nm (Fig. 3C).

3.1.4. FTIR spectra of PTO

Fig. 4 shows the FTIR spectra of PTO before and after EY and NBB degradation study. Peaks at 1565, 1487, 1306 and 1143 cm^{-1} are the peaks of quinonoid ring vibration, benzenoid ring vibration, C—N stretching and —NH^+= stretching vibration of PANI, respectively [52]. The general nature of the PTO before and after degradation and adsorption remained unchanged, which implies that after degradation and adsorption, the structure of PTO is unaltered, which in turn confirms about stable coating of TiO_2 by PANI.

3.1.5. XRD pattern of PANI-TiO_2

The X-ray diffraction (XRD) spectra of PTO was recorded at room temperature using a powder diffractometer (Rigaku) employing the CuK_α radiation (λ = 0.154 nm). The scans were performed at a 2θ = 10–80° at a scan rate of 1°/min and shown in Fig. S3 (supplementary materials). The prevalent peaks are at 25.3°, 27.7°, 36.1°, 37.7°, 41.2°, 48.0°, 54.3°, 62.8°, 69.06° and 75.1° which are all signature peaks of anatase phase of TiO_2 [53]. The strongest peak at 2θ = 25.3° is due to 101 plane of anatase TiO_2 which is merged with the peak of PANI at 2θ = 25.30°.

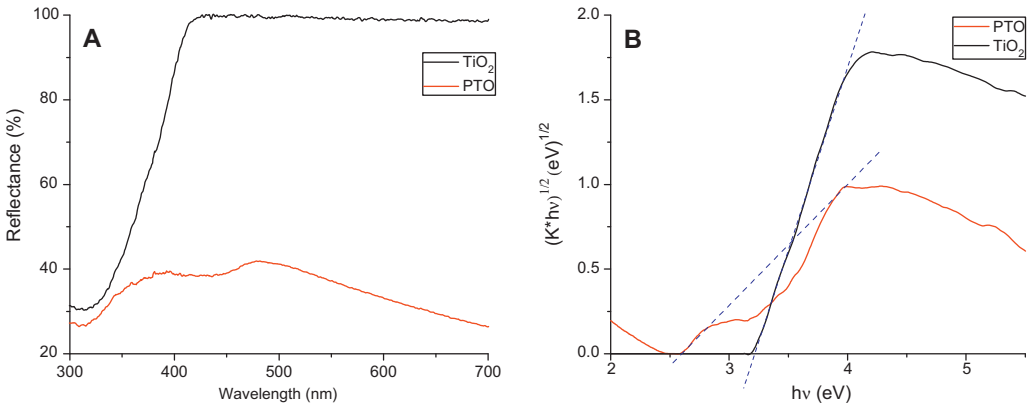

Fig. 2. (A) Diffuse reflectance UV–visible spectra and (B) Tauc plot for band gap energy of TO and PTO.

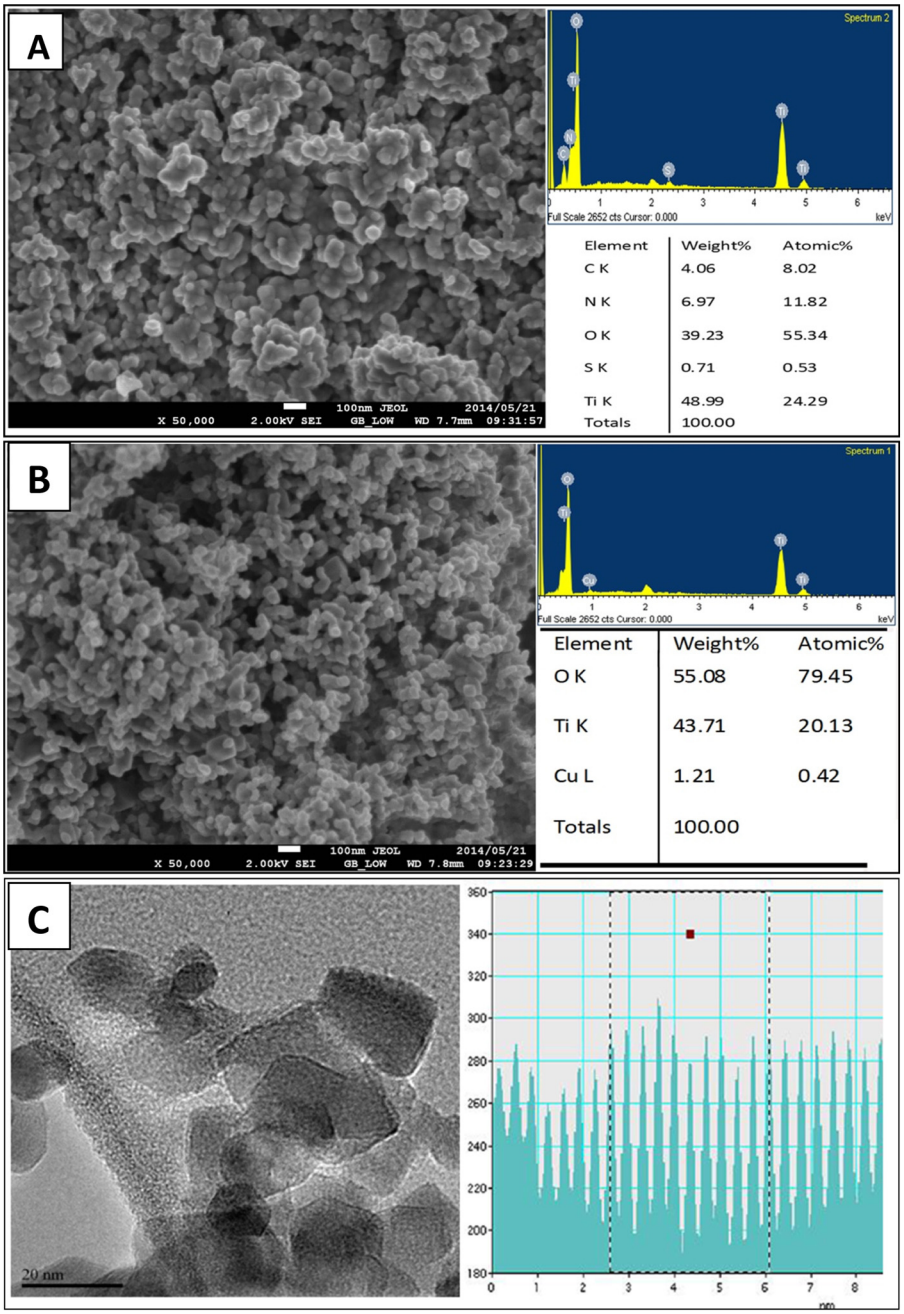

Fig. 3. SEM image and EDS spectra of (A) PTO, (B) TO and (C) TEM image of PTO and inter lattice distance of PTO particles.

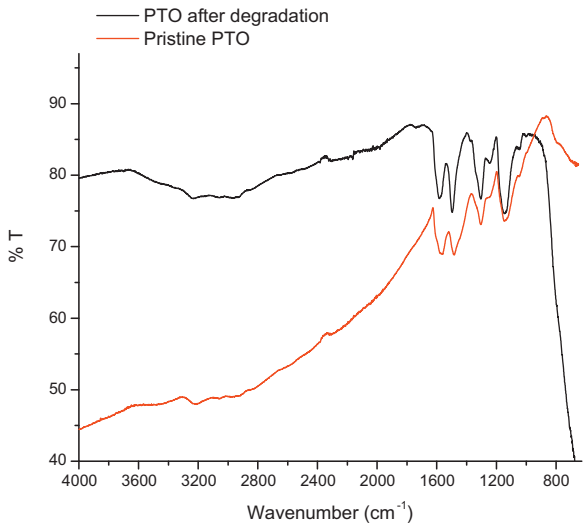

Fig. 4. FTIR spectra of PTO and before and after degradation.

3.1.6. Point of zero charge (pH_{zpc}) of the catalyst

Point of zero charge of the material was determined by zeta potential measurement and the pH vs zeta potential along with the change of phase plot is given in Fig. S4 (supplementary materials). The point of zero charge (pH_{zpc}) value of TO and PANI are 6.5 [53] and 8.49 (Fig. S5 (supplementary materials)), respectively. The surface of PANI is positively charged due to the dissociation of doped SO_4^- ions in PANI with simultaneous protonation of the nitrogen atoms of the polymer matrix in the presence of adequate H^+ ions [54]. As a composite consisting of PANI and TO, the pH_{zpc} of PTO was found to be 7.71, which is the combined effect shown by the composite. The increase in point of zero charge is more favorable for the adsorption of anionic dyes to the catalyst surface or closer to the surface where the degradation takes place.

3.1.7. UV–visible spectroscopy study of degradation of EY and NBB

Fig. S6 (supplementary materials) shows the UV–visible spectra of (A) EY and (B) NBB degradation with time. The spectra shows that the large peak at λ_{max} = 520 and 620 nm for EY and NBB, respectively, decreased gradually with the course of reaction time. The peaks below 300 nm, which are due to organic moieties present in the reaction solution also decreased with time, which indicates removal of organic compounds from the reaction solution.

3.1.7.1. Actinometric determination of the light intensity of the UV lamps. The light intensity of the UV lamps was determined by the ferrioxalate actinometer method [35]. The light intensity were found to be 13.11 and 14.35 mJ cm^{-2} min^{-1} for 15 W and 25 W lamps, respectively. Fig. S6 (supplementary materials) shows the performance of the ferrioxalate actinometer under the influence of both lamps.

3.2. Effect of pH of the solution

Degradations of EY and NBB by PTO nano-composite were investigated at pH 3.0, 6.2 and 11.0 (Fig. 5). The pH of the solution of the dye has a great influence on degradation study [55]. The degradation of the dyes are higher in acidic solution (pH 3.0) as well as in neutral solution (pH 6.2) than in basic solution (pH 11.0). Both EY and NBB are anionic dyes due to presence of carboxylate and sulfonate groups, respectively. The dyes are adsorbed more by the positively charged PTO surface at pH 3.0 and 6.2 and hence the degradation efficiency is higher at these two pHs (Table 2). Degradation is increased due to the fact that the hydroxyl radical (•OH) density is presumably more at the catalyst surface where it forms, which decreases into the bulk of the solution. On the other hand, the catalyst surface also exerts a negatively charged surface at the solution pH > pH_{zpc}. Hence, coulombic repulsion between the dye anions and the negatively charged catalyst surface decreases the adsorption of the dyes onto the catalyst surface. Moreover, presence of large excess of OH^- ions at high pH hinders the formation of hydroxyl radical formation [4] as well as competing with anionic dyes to adsorb on the surface of PTO.

3.3. Effect of photocatalyst dosage

Effects of catalyst dosage on degradation of EY and NBB were observed by adding 0.25, 0.5 and 1.0 g of the PTO catalyst in the reactor to 1 L of EY and NBB solution at pH 6.2 with initial concentration of 30.0 mg L^{-1}. The catalyst dosage was chosen in accordance to the conditions used in RSM optimization of degradation. Fig. 6 shows that with increase in catalyst dosage the degradation rate increases, which is a characteristic of heterogeneous photocatalysis [56]. With increase in catalyst dosage, the available active sites on the catalyst responsible for the generation of hydroxyl radical (•OH) increases and as a result the rate of degradation is also increased. This observation is supported by the rate constants calculated using Langmuir–Hinshelwood and second order kinetic models (Table 2). Both the rate constants (k_2 and k_{LH}) increase with increasing catalyst dosage, which implies the rate of degradation as well as adsorption (prevalent from increase in k_2), is also faster with high adsorbent dosage. The half life of the intermediates decreases with increasing catalyst dosage which implies that the intermediates are degraded very fast to the mineralization of the dye molecules [57].

3.4. Effect of influent dye concentration

The effect of initial dye concentration on degradation by PTO nanocomposite is shown in Fig. 7. Here, 0.5 g of the catalyst in 1 L of dye solutions of different initial concentration (15, 30 and 60 mg L^{-1}) was passed into the reactor at a flow rate of 10 mL min^{-1} under the 25 W UV lamp irradiation. As the initial concentration of the dye increase, the number of dye molecule also increase at a fixed number of active photo-catalyst sites. Thus, the rate of the degradation decreases. The results are shown in Table 2. A two fold increase in the rate constant of the reaction and the half life of intermediaries is observed when the initial dye concentration decreases two fold.

3.5. Effect of UV light intensity

To investigate the effect of UV light intensity on degradation of EY and NBB by the catalyst, two UV lamps of power 15 W and 25 W were employed with initial EY and NBB concentration of 30 mg L^{-1}. The experiments were conducted in the presence of light only without adsorbent and with presence of adsorbent in absence of light (Fig. 8). The results show that, with increase in UV light intensity from 15 W to 25 W, in case of EY, the rate of degradation increases from 0.016 to 0.027 min^{-1} and from 0.012 to 0.023 min^{-1}, in case of NBB. The increase in degradation rate is due to increase in generation of more number of •OH on the catalyst surface in presence of higher intense light. In the absence of a catalyst and the presence of UV light, the degradation rate is abnormally low with very high half-life. This indicates that there may be some bond breaking of the dye molecules in the presence of UV light with no effective decrease in dye concentration. In the presence of catalyst in the system without UV light (in dark), the decrease in color is due to adsorption only (R^2 for second order model = 0.9207 and 0.9124)

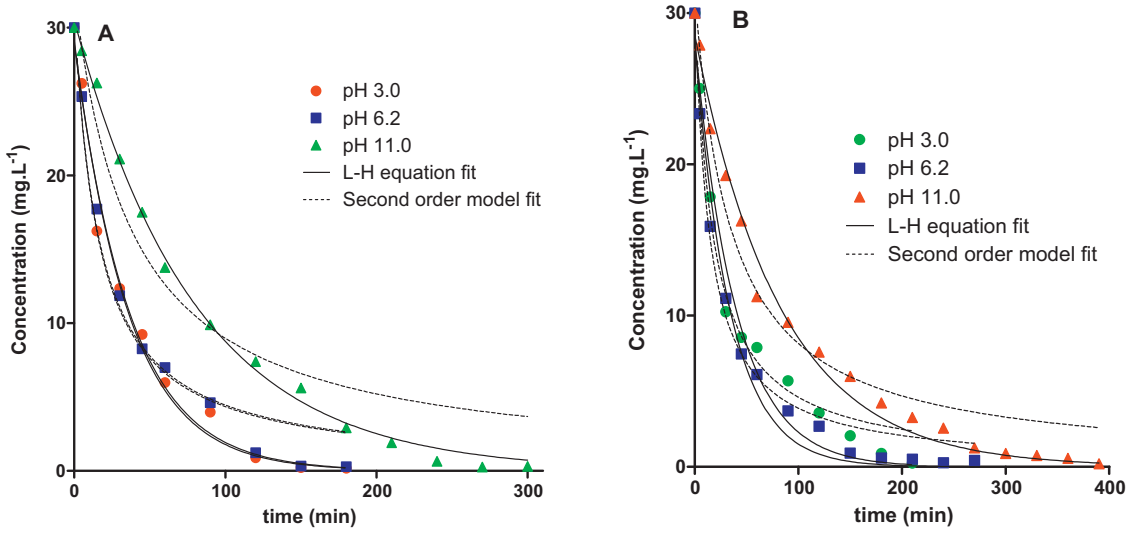

Fig. 5. Effect of pH on (A) EY and (B) NBB degradation by PTO in presence of UV light.

Table 2
The effect of key parameters on the rate of degradation of EY and NBB using PTO nanocomposite.

Parameters	$k_{LH} \times 10^{-3}$ (min^{-1})		R^2		$k_2 \times 10^{-4}$ (mg g^{-1} min^{-1})		R^2		Half life ($t_{1/2}$) (min)	
	EY	NBB	EY	NBB	EY	NBB	EY	NBB	EY	NBB
Concentration (mg L^{-1})										
15	56.43	85.85	0.9815	0.9836	78.52	131.1	0.9788	0.9864	10.46	6.48
30	27.11	29.18	0.9893	0.9624	19.35	22.53	0.9744	0.9929	23.45	20.96
60	23.54	16.03	0.9930	0.9599	8.63	6.76	0.9753	0.9873	27.01	33.00
Catalyst dosage (g L^{-1})										
0.25	11.17	10.3	0.9928	0.9877	7.59	7.99	0.9462	0.9474	69.08	102.7
0.50	27.11	29.2	0.9903	0.9836	19.61	22.51	0.9726	0.9864	24.00	30.24
1.00	49.95	36.9	0.9923	0.9834	36.18	28.82	0.9568	0.9708	13.60	25.68
pH										
3.0	27.92	25.10	0.9864	0.9676	19.82	18.48	0.9683	0.9847	23.42	21.33
6.2	27.13	29.18	0.9893	0.9836	19.35	22.53	0.9744	0.9864	23.45	20.96
11.0	12.54	12.07	0.9970	0.9887	8.06	9.07	0.9426	0.9707	59.91	51.60
Light intensity										
15 W	16.63	12.51	0.9926	0.9904	11.65	9.08	0.9664	0.9742	37.99	47.87
25 W	27.16	23.49	0.9893	0.9886	19.32	16.82	0.9744	0.9784	23.45	26.17
Dark	4.16	4.52	0.9839	0.9813	2.53	2.83	0.9207	0.9124	288.1	278.2
25 W w/o PTO	4.77	4.97	0.9900	0.9898	3.53	3.77	0.9598	0.9725	150.9	125.7

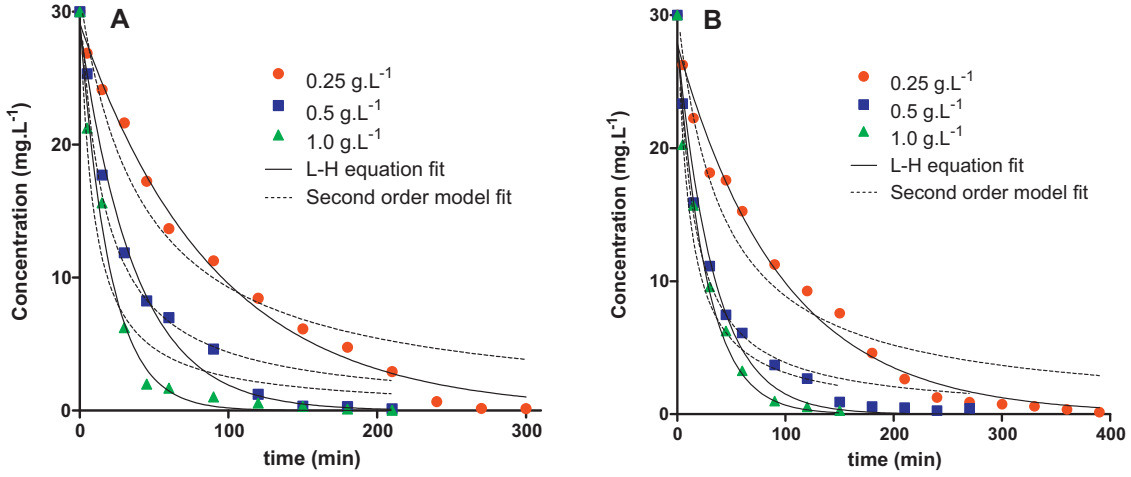

Fig. 6. Effect of dosage of PTO on (A) EY and (B) NBB degradation in presence of UV light.

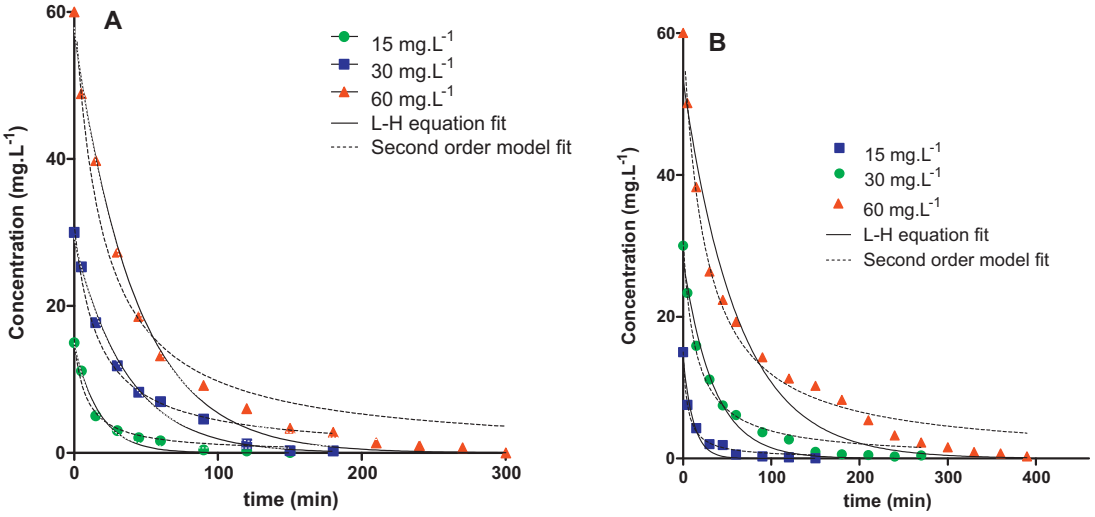

Fig. 7. Effect of initial concentration of (A) EY and (B) NBB on degradation efficiency by PTO in presence of UV light.

(Table 2), which indicates that adsorption on the catalyst surface is the major phenomena in this case rather than degradation.

3.6. Analysis of variance (ANOVA) and statistical analysis

Table 3 shows the results of the RSM fitting of the experimental data set in the form of analysis of variance (*ANOVA*). The *'F' value* and the *Prob. > F value* are the main indicators which determines the significance and the adequacy of the model [34]. The *Prob. > F* less than 0.05 indicate the model to be suitable one and greater than 0.1 is considered to be of less importance [58]. The *ANOVA* of this model for both the dyes used for degradation study (EY and NBB) demonstrated that the parameters are highly significant, which is evident from the low *'F' value* (32.00 and 15.84 for EY and NBB, respectively) and very low *Prob. > F* (<0.001) for the model. The very low *P* value indicates that the model can be considered significant and adequate to express the experimental data. The response of initial concentration (C_o), pH of the solution (*pH*), photocatalyst dosage (*m*), $C_o \times m$, $pH \times m$, pH^2 and m^2 for EY degradation are all found to be significant, which is evident from their Prob. > *F* value less than 0.05 (Table 3). In case of NBB the significant terms are C_o, *pH*, *m*, $C_o \times pH$, $pH \times m$, *and* m^2.

The relationship of the approximated function of the response of degradation with the varibale parameters is developed and expressed in terms of coded factors and actual factors and are given as Eqs. (1) and (2), for EY and Eqs. (3) and (4), for NBB, respectively, where *Y* is the degradation percentage after 150 min of UV irradiataion in the reactor.

$$\text{EY degradation \% (Y) (coded factor)} = 98.62 - 2.81X_1 - 11.20X_2 + 9.43X_3 - 1.51X_1X_2 + 2.21X_1X_3 + 5.93X_2X_3 + 0.39X_1^2 - 4.16X_2^2 - 11.87X_3^2 \quad (1)$$

$$\text{EY degradation \% (Y) (actual factor)} = 81.57 - 0.23X_1 - 0.99X_2 + 93.12X_3 - 0.017X_1X_2 + 0.26X_1X_3 + 3.95X_2X_3 + 7.69 \times 10^{-4}X_1^2 - 0.26X_2^2 - 84.38X_3^2 \quad (2)$$

$$\text{NBB degradation \% (Y) (coded factor)} = 94.78 - 4.93X_1 - 12.69X_2 + 10.21X_3 - 3.43X_1X_2 + 1.93X_1X_3 + 6.03X_2X_3 - 0.087X_1^2 - 3.14X_2^2 - 9.80X_3^2 \quad (3)$$

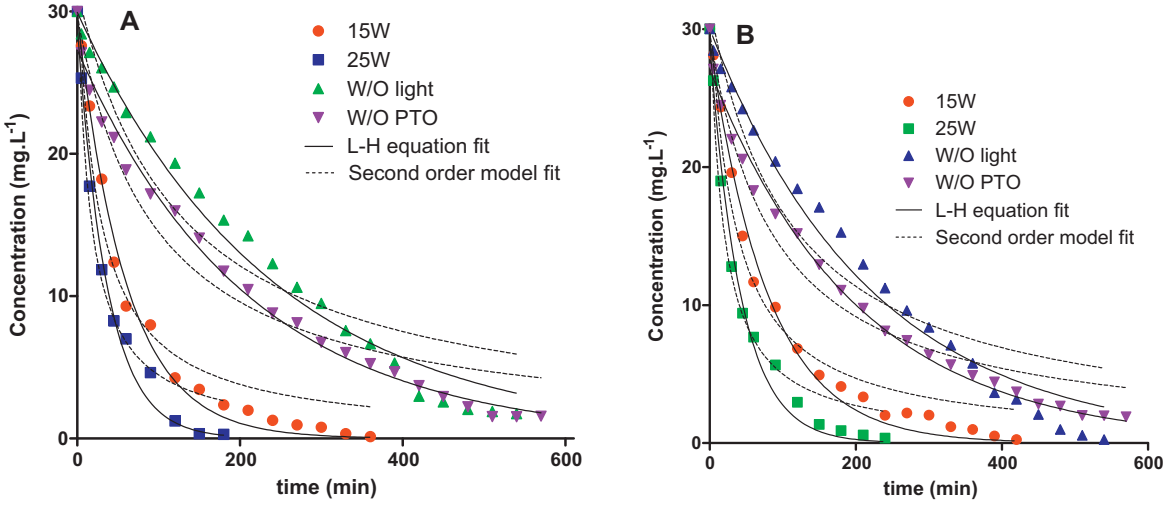

Fig. 8. Effect of intensity of UV light on degradation of (A) EY and (B) NBB by PTO.

Table 3
Analysis of variance of the developed quadratic model for EY and NBB degradation by PTO in presence of UV light.

Sources of variation	Sum of squares		Degree of freedom		Mean square		*F* value		Probability > F	
	EY	NBB	EY	NBB	EY	NBB	EY	NBB	EY	NBB
Model	3478.66	3974.88	9	9	386.52	441.65	32.00	15.84	<0.0001	<0.0001
C_o	78.11	241.46	1	1	78.11	241.46	6.46	8.65	0.0292	0.0147
pH	1240.32	1594.80	1	1	1240.32	1594.80	102.67	57.19	<0.0001	<0.0001
M	882.17	1033.94	1	1	882.17	1033.94	73.02	37.07	<0.0001	0.0001
$C_o \times pH$	18.90	97.37	1	1	18.89	97.37	1.56	3.49	0.2395	0.0912
$C_o \times m$	40.79	31.04	1	1	40.78	31.049	3.37	1.11	0.0960	0.3161
$pH \times m$	291.11	300.79	1	1	291.11	300.79	24.09	10.71	0.0006	0.0082
C_o^2	0.32	0.016	1	1	0.3195	0.016	0.026	0.0006	0.8740	0.9813
pH^2	41.09	23.42	1	1	41.09	23.42	3.40	0.84	0.0949	0.3810
m^2	296.43	202.25	1	1	296.43	202.25	24.53	7.25	0.0006	0.0226
Lack of fit	120.80	278.84	5	5	24.16	55.77				
Pure error	0.000	0.00	5	5	0.000	0.00				
Residual	120.80	278.84	10	10	12.08	27.88				
Total	3599.46	4253.73	19	19						

Table 4
Coefficient of regression and standard errors.

Source	Regression coefficient		Standard error	
	EY	NBB	EY	NBB
Constant	98.62	94.78	1.50	2.28
C_o	−2.80	−4.93	1.10	1.68
pH	−11.19	−12.69	1.10	1.69
m	9.43	10.21	1.10	1.68
$C_o \times pH$	−1.51	−3.43	1.20	1.84
$C_o \times m$	2.21	1.93	1.20	1.83
$pH \times m$	5.93	6.03	1.21	1.83
C_o^2	0.39	0.08	2.39	3.64
pH^2	−4.16	−3.14	2.25	3.43
m^2	−11.87	−9.80	2.39	3.64

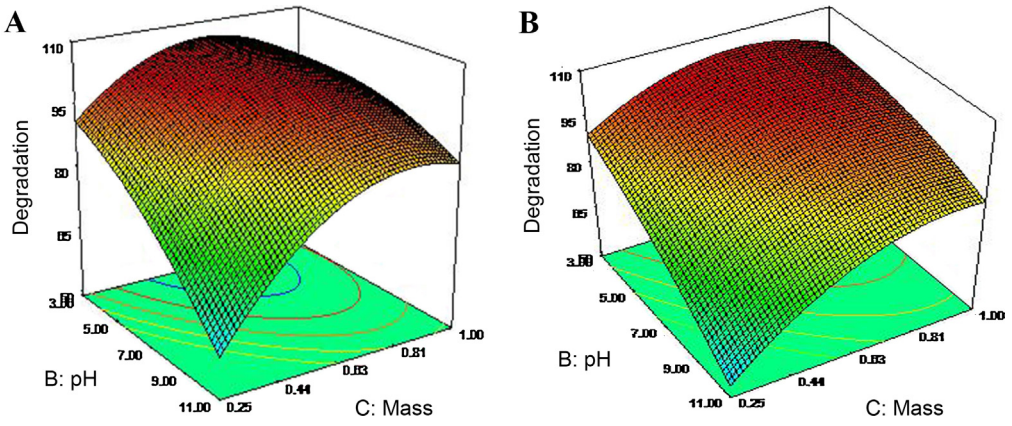

Fig. 9. Response surface plots showing the effect of independent variables catalyst mass and pH on degradation of (A) EY and (B) NBB by PTO under UV light.

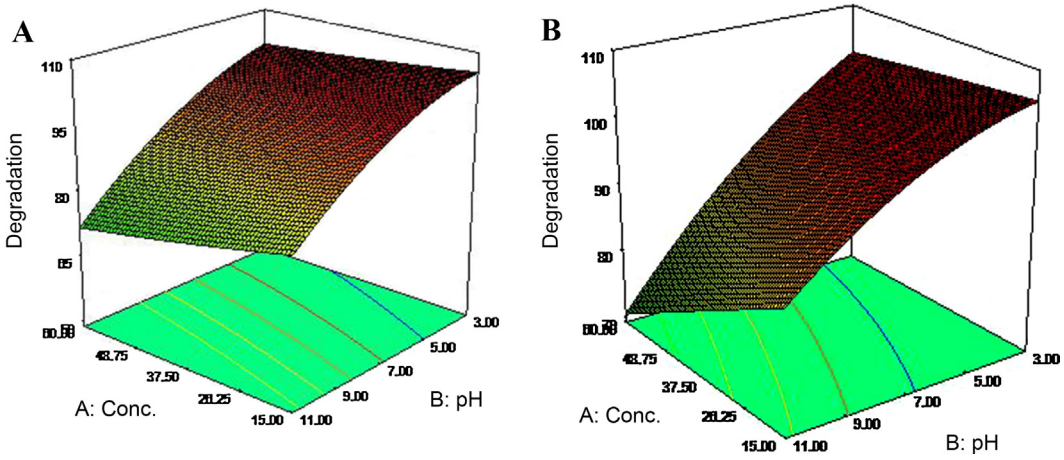

Fig. 10. Response surface plots showing the effect of independent variables initial dye concentration and pH on degradation of (A) EY and (B) NBB by PTO under UV light.

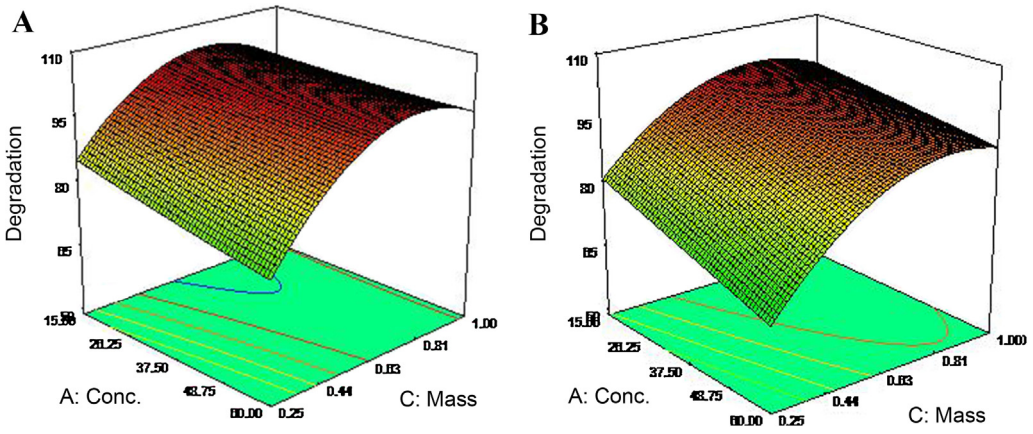

Fig. 11. Response surface plots showing the effect of independent variables initial dye concentration and catalyst mass on degradation of (A) EY and (B) NBB by PTO under UV light.

$$\text{NBB degradation \% (Y) (actual factor)} = 84.04 - 0.08X_1 - 1.51X_2 + 77.65X_3 - 0.038X_1X_2 + 0.22X_1X_3 + 4.02X_2X_3 - 1.73 \times 10^{-4}X_1^2 - 0.19X_2^2 - 69.69X_3^2 \quad (4)$$

The signs and the magnitudes of the regression coefficients are the representative of the each variable on the response. A positive sign indicates that the individual variable or the interacted variables has synergistic effect on the response, whereas, the negative sign indicates the antagonistic effect on the response [59]. As observed from Table 4, the concentration and pH has antagonistic effect but catalyst dosage has synergistic effect on the degradation. The term with the highest regression coefficient is the pH, which indicates that in the overall response, pH is the dominant factor. Specifically, for both the dyes the pH value below the center

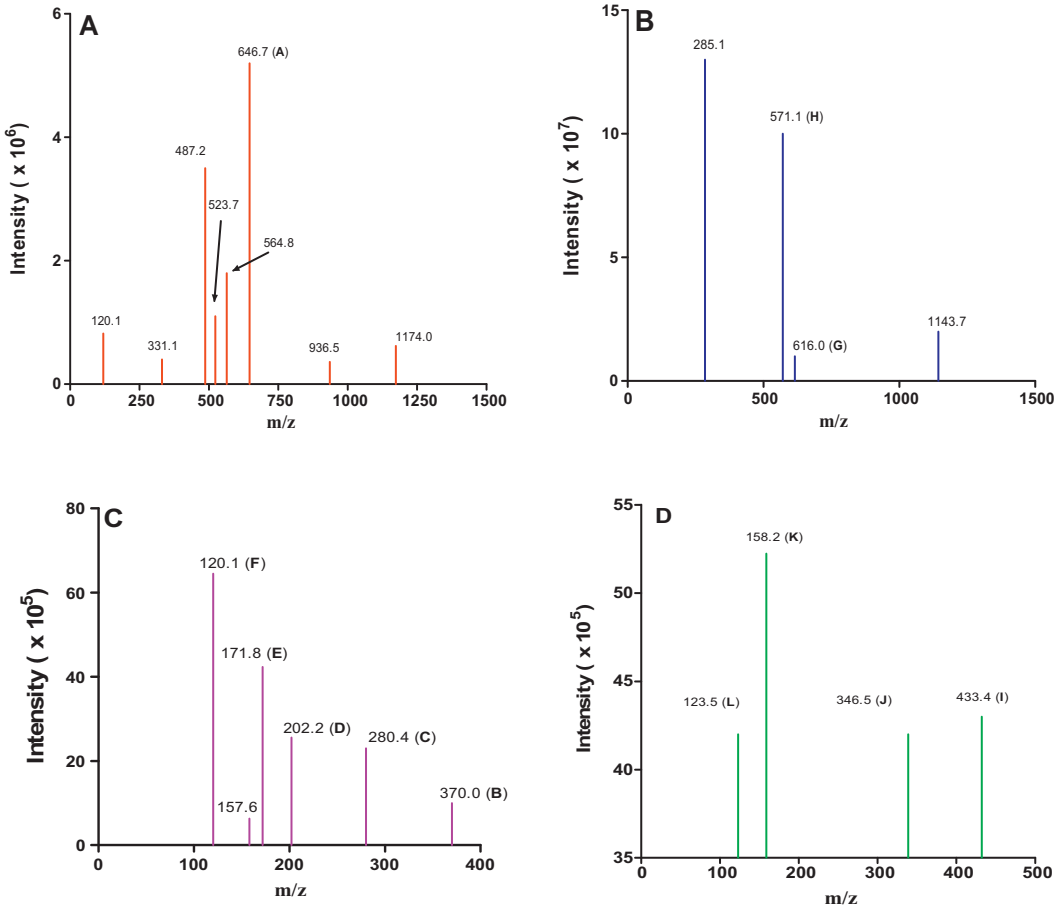

Fig. 12. The LCMS spectra of the (A) EY before UV irradiation, (B) NBB before UV irradiation, (C) EY after 180 min UV irradiation and (D) NBB after 180 min irradiation in presence of PTO.

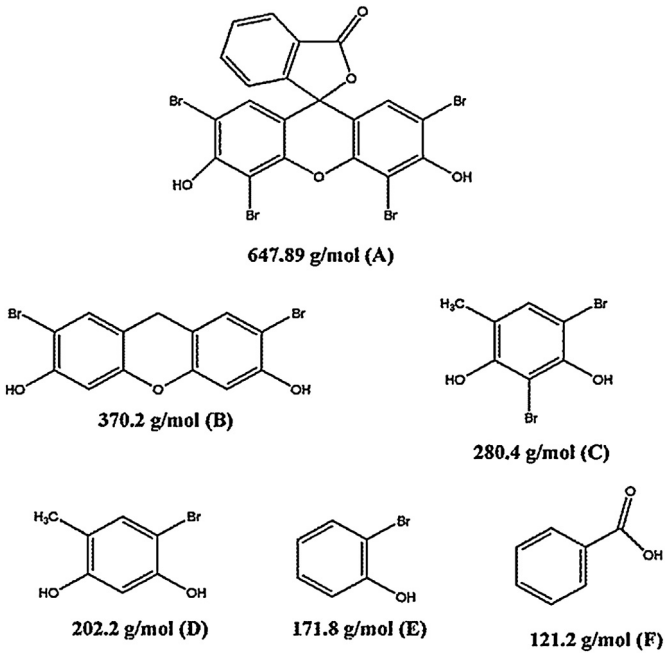

Scheme 1. Possible degradation products of EY after UV irradiation in presence of PTO, as determined by LC–MS spectrum given in Fig. 12A and C. Letters in parentheses are the species identified in Fig. 12A and C.

point of the experimental design correspond to the highest degree of degradation. Similarly, m has also high synergistic regression coefficient for both the dyes. This indicates that the m above the center point of the experimental design has highest degree of degradation efficiency. These results are consistent with the Fig. 6A and B.

3.7. Optimization of degradation of EY and NBB by PTO under UV irradiation using RSM

The three dimensional response surface plots were analyzed to observe the better insight of the degradation of the dyes by PTO. In each plot two variables are varied while the other varibale was kept constant. The response surface plots for EY and NBB degradation are shown in Figs. 9–11. In degradation study, the pH and the catalyst dosage are the most influential variables.

Fig. 9 shows the simultaneous effect of pH and the adsorbent dosage on degradation of (A) EY and (B) NBB. With decrease in pH and increase in adsorbent dosage, the degradation percentage increases. This is likely the result of more active surface sites at higher catalyst dosage and increased surface positive charge at lower pH (both the dyes are anionic). This synergestic effect of the cross interaction term ($pH \times m$) justifies the observation of the positive regression coefficient of the RSM analysis (Table 4).

Fig. 10 demonstrates the simultaneous effect of initial dye concentration and pH on degradation. With increase in initial concentration the number of dye molecule per unit surface of the catalyst increases and this results in lower percentage of degradation. The increased pH value also does not favors the generation of the hydroxyl radical (•OH). These effects confirm the anatagonistic effect of the cross interaction term of C_o and pH ($C_o \times$ pH) in the regression analysis.

Fig. 11 demonstrates the interaction of initial dye concentration with the catalyst dosage. The C_o individually has the antagonistic effect on the degradation. However, the cross interaction term of C_o and adsorbent dosage (m) ($C_o \times m$) has synergistic effect on degradation (Table 4). The magnitude of m is relatively higher than the magnitude of the C_o. Thus the antagonistic effect of the C_o is suppressed by the synergistic effect of m and as a result the overall effect of the cross interaction between C_o and m ($C_o \times m$) becomes synergistic. Physically, this can be attributed to the fact that with

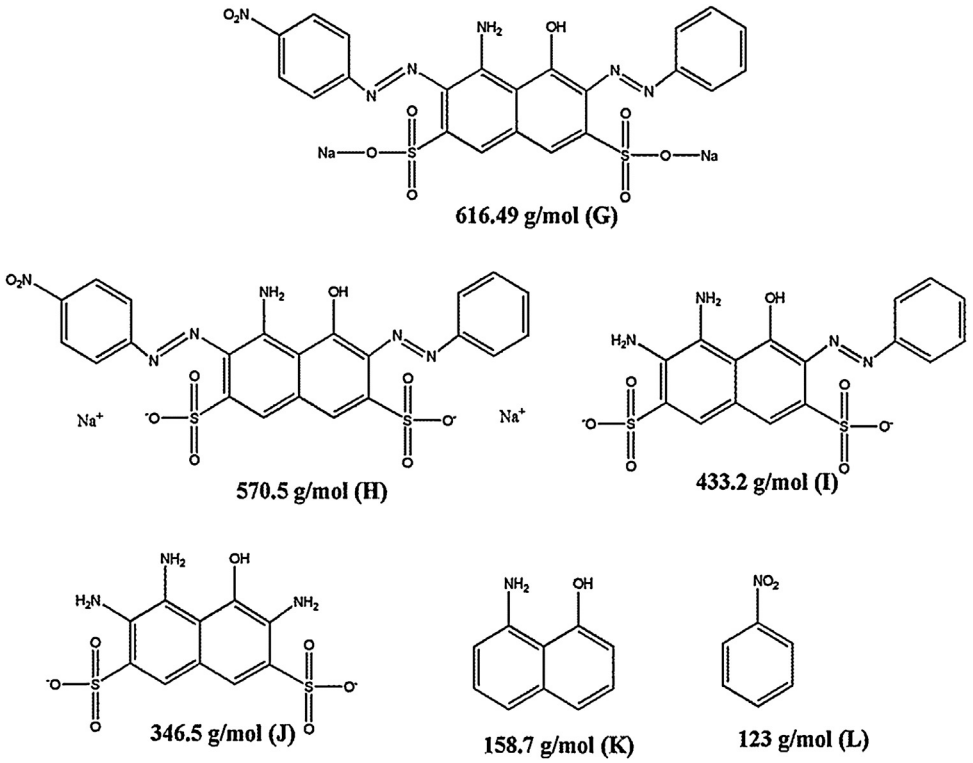

Scheme 2. Possible degradation products of NBB after UV irradiation in presence of PTO, as determined by LC–MS spectrum given in Fig. 12B and D. Letters in parentheses are the species identified in Fig. 12B and D.

increased catalyst dosage the active surface sites are so increased with respect to the increased dye molecules at increased C_o, the effect on degradation becomes positive.

By using the response surface design and optimization, for EY the optimum degradation percentage (99.85) was obtained at pH 3.0, initial dye concentration 15 mg L^{-1} and catalyst dosage 1.0 g L^{-1}. For NBB, the optimum degradation percentage (99.74) was also obtained at pH 3.0, initial dye concentration 15 mg L^{-1} and catalyst dosage 1.0 g L^{-1}.

3.8. Determination of the degraded products by LCMS study and proposed mechanism of the degradation

The degraded products and the intermediaries formed during the course of the degradation study were identified by the LC–MS analyses and their mass spectra were interpreted from their molecule ion peaks with respect to the *m/z* ('*m*'; the molecular weight of the intermediaries in the mass spectra). The mass spectra of the solution of EY and NBB before degradation are given in Fig. 12A and B, respectively. The molecular peak of un-ionized EY (*m/z* = 646.7) is the main peak in Fig. 12A, indicating the presence of un-degraded and prevalently un-ionized form of EY in the initial solution. The other peaks present in the spectra are the representative of the ionized or the adduct product of the mother molecule.

The molecular peak of un-ionized form (*m/z* = 616.0) is not the major peak in the initial NBB solution. The NBB remains mainly in ionized form in the initial NBB solution, which is evident from the presence of two peaks (*m/z* = 571.1 and 285.1).

Fig. 12C and D shows the degradation products of EY and NBB after 180 min of UV irradiation. The molecular peaks of the non-degraded dye molecule are not observed at all. Although, the molecular peak of un-ionized peaks of NBB was not visible in the LCMS of the dye before irradiation, the peaks of the ionized form of the non-degraded forms were also invisible in the LCMS of the product after 180 min of irradiation. This means that the NBB molecule also undergoes degradation under UV irradiation.

The spectrum of EY and NBB in Fig. 12A and B, respectively, are different from the spectra of the irradiated EY and NBB in Fig. 12C and D, respectively. The difference can be explained due to the decomposition of the dyes in different *m/z* in the presence of PTO.

The peaks at *m/z* ratio 646.6 and 487.2 in the spectrum of non-irradiated EY (Fig. 12A) were not observed in the spectrum of the irradiated EY (Fig. 12C). Similarly, the peaks in the spectrum of non-irradiated NBB (Fig. 12B) at *m/z* ratio 285.1, 571.1 and 616.0 were not visible in the spectrum of the irradiated NBB (Fig. 12D). The disappearance of these peaks therefore confirms that degradation occurred under UV radiation.

The degradation of both the dyes can be initiated by the available $OH^{\bullet}$ generated from the catalyst (PTO). The degradation of the dyes may occur through the following steps, (i) the cleavage of the aryl ring (specifically, the benzene rings at the sides of the molecules decomposes, (ii) the ionization of the dye molecules in aqueous solution (iii) cleavage of the C—S bond in NBB (iv) cleavage of various C—O, C—N and C—C bond by the attack of the $OH^{\bullet}$ and (iv) —N=N— double bond cleavage.

According to the results obtained from the LCMS data, the following schemes (Schemes 1 and 2) were proposed for the degradation of EY and NBB in presence of PTO under UV light.

4. Conclusion

A polyaniline-coated titanium dioxide nanocomposite (PTO) was successfully synthesized, characterized and used as a catalyst in the photo-degradation of the dyes EY and NBB. The degree of degradation increases at lower pH; increasing catalyst dosage and increasing initial dye concentrations. The effect of UV light intensity in the absence of the catalyst is not significant. Langmuir–Hinselwood and second order kinetic models have provided evidence for a heterogeneous photo-catalysis. The response-surface statistical analysis revealed that the combined effect of pH and initial dye concentration is antagonistic. Contrarily, the combined effects of catalyst dosage and pH and the combined effect of catalyst dosage and initial dye concentration are synergistic. This suggests that catalyst dosage is the most significant process parameter governing the degradation process. The optimum degradation percentages were evaluated as 99.85 and 99.74 for EY and NBB, respectively. This was achieved at pH 3.0, initial dye concentration of 15 mg L^{-1} and a catalyst dosage of 1.0 g L^{-1}. These preliminary results therefore suggest that PTO is an efficient catalyst for the degradation of EY and NBB, if the optimum conditions of pH, initial dye concentration and catalyst dosage were maintained. A LC–MS analysis confirmed that degradation occurred after UV irradiation and the photodegradation products were identified and provide experimental evidence for the generation of a hydroxyl radical and decomposition of benzene ring followed by ionization of the dye molecules and cleavage of C—S, C—C, —N=N— and C—N bonds by the hydroxyl radical.

Acknowledgment

The authors are grateful to HOD, Department of Applied Chemistry, University of Johannesburg, for providing infrastructural facility and Water Research Commission (WRC) (Grant No. 1003392), South Africa and Eskom, South Africa for financial support. The authors are also grateful to Council for Scientific and Industrial Research (CSIR), South Africa for providing research infrastructures to this project..

Appendix A. Supplementary data

Supplementary data associated with this article can be found, in the online version, at http://dx.doi.org/10.1016/j.apcatb.2014.08.011

References

[1] R. Molinari, F. Pirillo, M. Falco, V. Loddo, L. Palmisano, Chem. Eng. Process.: Process Intensif. 43 (2004) 1103–1114.
[2] S. Bilgi, C. Demir, Dyes Pigments 66 (2005) 69–76.
[3] I.K. Konstantinou, T.A. Albanis, Appl. Catal. B—Environ. 49 (2004) 1–14.
[4] S. Song, L. Xu, Z. He, H. Ying, J. Chen, X. Xiao, B. Yan, J. Hazard. Mater. 152 (2008) 1301–1308.
[5] R.O.A. Lima, A.P. Bazo, D.M.F. Salvadori, C.M. Rech, D.P. Oliveira, G.A. Umbuzeiro, Mutat. Res./Genet. Toxicol. Environ. Mutagen. 626 (2007) 53–60.
[6] P.A. Carneiro, G.A. Umbuzeiro, D.P. Oliveira, M.V. Zanoni, J. Hazard. Mater. 174 (2010) 694–699.
[7] F.M.D. Chequer, T.M. Lizier, R. de Felicio, M.V.B. Zanoni, H.M. Debonsi, N.P. Lopes, R. Marcos, D.P. Oliveira, Toxicol. Vitro 25 (2011) 2054–2063.
[8] D.P. Oliveira, P.C.A. Carneiro, M.K. Sakagami, M.V. Zanoni, G.A. Umbuzeiro, Mutat. Res./Genet. Toxicol. Environ. Mutagen. 626 (2007) 135–142.
[9] S. Venitt, C.C. Sleigh, M.R. Osborne, Mutat. Res./Genet. Toxicol. 135 (1984) 31–47.
[10] C. Tang, V. Chen, Water Res. 38 (2004) 2775–2781.
[11] A. Akyol, H.C. Yatmaz, M. Bayramoglu, Appl. Catal. B—Environ. 54 (2004) 19–24.
[12] C.A.K. Gouvea, F. Wypych, S.G. Moraes, N. Duran, N. Nagata, P.P. Zamora, Chemosphere 40 (2000) 433–440.
[13] M.A. Adebayo, L.D.T. Prola, E.C. Lima, M.J.P. Rosero, R. Catalua, C. Saucier, C.S. Umpierres, J.C.P. Vaghetti, L.G. da Silva, R. Ruggiero, J. Hazard. Mater. 268 (2014) 43–50.
[14] A. Afkhami, R. Moosavi, J. Hazard. Mater. 174 (2010) 398–403.
[15] Z. Aksu, G. Donmez, Chemosphere 50 (2003) 1075–1083.
[16] S. Bai, X. Shen, X. Zhong, Y. Liu, G. Zhu, X. Xu, K. Chen, Carbon 50 (2012) 2337–2346.
[17] C. Guillard, H. Lachheb, A. Houas, M. Ksibi, E. Elaloui, J.M. Herrmann, J. Photochem. Photobiol. A: Chem. 158 (2003) 27–36.
[18] C. Hachem, F. Bocquillon, O. Zahraa, M. Bouchy, Dye Pigments 49 (2001) 117–125.

[19] V. Augugliaro, C. Baiocchi, A. Bianco Prevot, E.G. Lopez, V. Loddo, S. Malato, G. Marci, L. Palmisano, M. Pazzi, E. Pramauro, Chemosphere 49 (2002) 1223–1230.
[20] C.C. Chan, C.C. Chang, W.C. Hsu, S.K. Wang, J. Lin, Chem. Eng. J. 152 (2009) 492–497.
[21] C.H. Chiou, C.Y. Wu, R.S. Juang, Chem. Eng. J. 139 (2008) 322–329.
[22] J. Kiwi, C. Pulgarin, P. Peringer, M. Gratzel, Appl. Catal. B: Environ. 3 (1993) 85–99.
[23] S. Tanaka, T. Ichikawa, Water Sci. Technol. 28 (1994) 103–110.
[24] A.K. Gupta, A. Pal, C. Sahoo, Dyes Pigments 69 (2006) 224–232.
[25] T.S. Natarajan, M. Thomas, K. Natarajan, H.C. Bajaj, R.J. Tayade, Chem. Eng. J. 169 (2011) 126–134.
[26] M. Anpo, S. Dohshi, M. kitano, Y. Hu, M. Takeuchi, M. Matsuoka, Annu. Rev. Mater. Res. 35 (2005) 1–27.
[27] M. Kanna, W. Sumpun, Mater. Chem. Phys. 110 (2008) 166–175.
[28] I.K. Konstantinou, T.A. Albanis, Appl. Catal. B: Environ. 49 (2004) 1–14.
[29] L. Wang, Z. Wang, D. Wang, X. Shi, H. Song, X. Gao, Solid State Sci. 31 (2014) 85–90.
[30] X. Guo, C. Chen, W. Song, X. Wang, W. Di, W. Qin, J. Mol. Catal. A: Chem. 387 (2014) 1–6.
[31] A. Tang, Y. Jia, S. Zhang, Q. Yu, X. Zhang, Catal. Commun. 50 (2014) 1–4.
[32] Y.C. Lin, H.S. Lee, J. Hazard. Mater. 179 (2010) 462–470.
[33] S. Wang, K.K. Meng, L. Zhao, Q. Jiang, J.S. Lian, Ceram. Int. 40 (2014) 5107–5110.
[34] P. Hou, F.S. Cannon, C. Nieto-Delgado, N.R. Brown, X. Gu, Chem. Eng. J. 223 (2013) 309–317.
[35] P.G. Hatchard, C.A. Parker, Proc. R. Soc. Lond. A235 (1956) 518–536.
[36] AWWA, APHA, WEF, Standard Methods for the Examination of Water and Wastewater, twentieth ed. Washington DC, 1998.
[37] L. Rizzo, S. Meric, D. Kassinos, M. Guida, F. Russo, V. Belgiorno, Water Res. 43 (2009) 979–988.
[38] Y. Liu, X. Chen, J. Li, C. Burda, Chemosphere 61 (2005) 11–18.
[39] D.C. Montgomery, Design and Analysis of Experiments, John Wiley & Sons, New York, 2001.
[40] R.H. Myres, D.C. Montgomery, Response Surface Methodology: Process and Product Optimization Using Designed Experiments, John Wiley and Sons, New York, 1995.
[41] A.L. Ahmad, S. Ismail, S. Bhatia, Environ. Sci. Technol. 39 (2005) 2828–2834.
[42] J. Kumar, A. Bansal, J. Environ. Chem. Eng. 1 (2013) 398–405.
[43] Z.M. Shaykhi, A.A.L. Zinatizadeh, J. Taiwan Inst. Chem. Eng. 45 (2014) 1717–1726.
[44] Il-H. Cho, K.D. Zoh, Dyes Pigments 75 (2007) 533–543.
[45] A. Zuorro, M. Fidaleo, R. Lavecchia, J. Environ. Manag. 127 (2013) 28–35.
[46] H. Muhamad, S.R.S. Abdullah, A.B. Mohamad, R.A. Rahman, A.A.H. Kadhum, J. Environ. Manag. 121 (30 May 2013) 179–190.
[47] MSDS of Aeroxide P25. ⟨http://www.acros.be/DesktopModules/Acros_Search_Results/Acros_Search_Results.aspx?search_type=CatalogSearch&SearchString=38429.2014⟩. Acros Organics.
[48] S. Sakthivel, H. Kisch, Angew. Chem. Int. Ed. 42 (2003) 4908–4911.
[49] A.P. Monkman, P. Adams, Solid State Commun. 78 (1991) 28–31.
[50] O. Kwon, M.L. McKee, J. Phys. Chem. B 104 (2000) 1686–1694.
[51] F. Wang, S. Min, Y. Han, L. Feng, Superlattice Microstruct. 48 (2010) 170–180.
[52] M.V. Kulkarni, B.B. Kale, Sens. Actuators B: Chem. 187 (2013) 407–412.
[53] S. Debnath, N.R. Roy, U.C. Ghosh, Int. J. Green Nanotechnol. 3 (2011) 271–280.
[54] M. Bhaumik, H.J. Choi, R.I. McKrindle, A. Maity, J. Colloid Interface Sci. 425 (2014) 75–82.
[55] E.K. Goharshadi, M. Hadadian, M. Karimi, H. Azizi-Toupkanloo, Mater. Sci. Semicond. Process. 16 (2013) 1109–1116.
[56] M.A. Rauf, M.A. Meetani, S. Hisaindee, Desalination 276 (2011) 13–27.
[57] I.H. Cho, K.D. Zho, Dyes Pigments 75 (2007) 533–543.
[58] N.B. Parilti, C.S.U. Demirel, M. Bekbolet, J. Photochem. Photobiol. A: Chem. 225 (2011) 26–35.
[59] K.P. Singh, S. Gupta, A.K. Singh, S. Sinha, J. Hazard. Mater. 186 (2011) 1462–1473.